Dark matter from phase transition generated PBH evaporation with gravitational waves signatures

Debasish Borah,[1,*] Suruj Jyoti Das,[2,†] and Indrajit Saha[1,‡]

[1]*Department of Physics, Indian Institute of Technology Guwahati, Assam 781039, India*
[2]*Particle Theory and Cosmology Group, Center for Theoretical Physics of the Universe, Institute for Basic Science (IBS), Daejeon 34126, Korea*

(Received 23 April 2024; accepted 18 July 2024; published 12 August 2024)

We study the possibility of generating dark matter (DM) purely from ultralight primordial black hole (PBH) evaporation with the latter being produced from a first order phase transition (FOPT) in the early Universe. If such ultralight PBH leads to an early matter domination, it can give rise to a doubly peaked gravitational wave (GW) spectrum in Hz-kHz ballpark with the low frequency peak generated from PBH density fluctuations being within near future experimental sensitivity. In the subdominant PBH regime, the FOPT generated GW spectrum comes within sensitivity due to absence of entropy dilution. In both the regimes, PBH mass from a few kg can be probed by GW experiments like BBO, ET, CE, UDECIGO etc. while DM mass gets restricted to the superheavy ballpark in the PBH dominance case. Apart from distinct DM mass ranges in the two scenarios, GW observations can differentiate by measuring their distinct spectral shapes.

DOI: 10.1103/PhysRevD.110.035014

I. INTRODUCTION

Primordial black holes (PBH), originally proposed in [1] and later by Hawking [2,3] can have several interesting cosmological consequences [4,5]. A recent review of PBH can be found in [6]. Depending upon the initial mass $(m_{\rm in})$ and initial energy fraction (β), PBH can face different astrophysical and cosmological constraints. Among them, the ultralight PBH mass window is relatively less constrained as such PBH evaporate by emitting Hawking radiation [2,3] before the big bang nucleosynthesis (BBN) epoch. Comparing the evaporation temperature with the BBN temperature $T_{\rm ev} > T_{\rm BBN} \simeq 4$ MeV leads to the upper bound on this ultralight PBH mass window. On the other hand, a lower bound can be obtained by using the upper limit on the scale of inflation from cosmic microwave background (CMB) measurements. Using these BBN and CMB bounds simultaneously leads to the allowed initial mass for ultralight PBH that reads $0.1\ {\rm g} \lesssim m_{\rm in} \lesssim 3.4 \times 10^8$ g. As mentioned above, the range of PBH masses in this window is relatively unconstrained [6]. It should be noted that the upper bound is obtained only for PBH which evaporates on a timescale smaller than the age of the universe and have a large initial fraction β to dominate the energy density at some epoch. Such evaporation of ultralight PBH can also lead to the production of dark matter (DM) in the universe [7–23]. As suggested by observations in astrophysics and cosmology based experiments, approximately 26% of the present universe is made up of DM, the particle origin of which is not yet known. If DM has only gravitational interactions as observations indicate, the conventional thermal freeze-out mechanism fails and PBH evaporation provides a very good alternative.

While DM with only gravitational interactions may not have much detection prospects, the ultralight PBH and their formation mechanisms in the early universe can lead to promising detection prospects. In spite of this relatively less constrained mass window, it is still possible to probe an ultralight PBH dominated epoch in the early universe via detection of stochastic gravitational waves (GW) background.[1] Interestingly, detection of stochastic GW can also probe the formation mechanism of PBH in the early universe. In the early universe, PBH can be formed in a variety of ways like, from inflationary perturbations [25–29], first-order phase transition (FOPT) [30–42], the collapse of topological defects [43,44] etc. Such mechanisms often come up with their own unique GW spectrum.

*Contact author: dborah@iitg.ac.in
†Contact author: surujjd@gmail.com
‡Contact author: s.indrajit@iitg.ac.in

[1]See Ref. [24] for a recent review on stochastic gravitational wave background.

On the other hand, PBH can lead to generation of GW in a variety of ways. The Hawking evaporation of PBH itself can produce gravitons which might constitute an ultrahigh frequency GW spectrum [45]. PBH can also lead to GW emission by forming successive mergers [46]. In addition, the scalar perturbations leading to the formation of PBH can induce GW at second-order [47], which can be further enhanced during the PBH evaporation [48]. Finally, the inhomogeneity in the distribution of PBH may also induce GW at second order, as recently studied in [49–51]. In the present work, we consider the last possibility which, for ultralight PBH mass window, can lead to stochastic GW with peak frequencies in the ballpark of ongoing and planned future experiments.

Motivated by this, we study the possibility of simultaneously probing the signatures of formation mechanism and PBH via detection of stochastic GW background with nontrivial implications for dark matter produced solely from PBH evaporation. Recently, FOPT origin of heavy PBH was studied by the authors of [52–57]. Here, we consider the ultralight PBH mass window, not considered in earlier works and study the possibility of forming them in FOPT. The combined GW spectrum arising out of the FOPT and density perturbations of ultralight PBH consists of a unique doubly-peaked feature. For the PBH mass range of interest, the peak in GW spectrum due to FOPT occurs at a frequency higher than the one due to PBH density perturbations. Depending upon the model parameters, the peak frequencies and corresponding blue and red tilted parts of the GW spectrum remain within the sensitivities of several planned experiments like DECIGO [58], BBO [59], ET [60], CE [61], UDECIGO (UDECIGO-corr) [62,63] etc. While doubly peaked GW spectrum arises in a scenario with PBH domination, the DM parameter space is typically restricted to the superheavy ballpark. In subdominant PBH scenario, DM mass range gets much wider whereas the GW spectrum generated by FOPT comes within the sensitivities of several future experiments. Depending upon the specific scenario, DM masses from GeV to superheavy regime and PBH mass as low as a few kg remains within sensitivities of such GW experiments. It is worth mentioning that in most of the earlier works studying DM production from PBH evaporation, the formation mechanism of the latter is not included. The inclusion of the PBH formation mechanism not only leads to a tighter parameter space but also to complementary detection prospects.

This paper is organized as follows. In Sec. II, we outline the particle physics setup responsible for FOPT followed by discussion of PBH formation in Sec. III. In Sec. IV and Sec. V, we discuss the stochastic GW generated by FOPT and PBH density fluctuations respectively. In Sec. VI, we discuss the combined GW spectrum arising from FOPT and PBH followed by implications for DM phenomenology in Sec. VII. We briefly comment on other FOPT origin of PBH not discussed in this work and the corresponding GW signatures in Sec. VIII. We finally conclude in Sec. IX.

II. THE SETUP

Among different scenarios relating FOPT to PBH formation [30–42], we consider the false vacuum collapse as the origin of PBH formation. In particular, we consider the collapsing Fermi-ball scenario [35,36,41,42,53,64–67]. In this scenario, a dark sector fermion χ with an asymmetry between χ and $\bar{\chi}$ leads to the formation of Fermi-balls after getting trapped in the false vacuum. Due to the strong Yukawa force among the dark fermions, such Fermi-balls can collapse into PBH. As the dark sector is asymmetric[2] and carries a conserved charge, we consider a global dark $U(1)_D$ symmetry which remains unbroken as the Universe goes through a FOPT. The dark sector fermion χ has a charge q_χ under this $U(1)_D$ global symmetry while all other fields are neutral. We consider the FOPT to be driven by a singlet scalar Φ. The dark sector fermion χ is coupled to Φ through Yukawa interaction. Since fermion and bosons contribute with opposite signs to the effective potential, and fermion χ has large Yukawa coupling with Φ, additional bosonic degrees of freedom are required to have an effective potential consistent with a strong FOPT while keeping all dimensionless couplings within perturbative limits. We consider an additional singlet scalar Φ' and doublet scalar H_2 for this purpose. However, this choice is arbitrary. For example, if we embed this setup within a new gauge symmetry under which Φ transforms nontrivially, such extra scalar fields are no longer required. These additional scalars are also neutral under $U(1)_D$ global symmetry and their couplings with Φ are the only relevant ones for our analysis.

The relevant Lagrangian of these newly introduced fields is given by

$$\mathcal{L} \supset -g_\chi \Phi \bar{\chi}\chi - m_\chi \bar{\chi}\chi - V(\Phi, \Phi', H_2) \tag{1}$$

where, the scalar potential (suppressing a few allowed terms for simplicity) is

$$\begin{aligned} V(\Phi, \Phi', H_2) = \lambda_D \left(|\Phi|^2 - \frac{v_D^2}{2} \right)^2 + m_{\Phi'}^2 |\Phi'|^2 + \lambda_{\Phi'} |\Phi'|^4 \\ + \lambda_{\Phi\Phi'} |\Phi|^2 |\Phi'|^2 + m_{H_2}^2 |H_2|^2 + \lambda_{H_2} |H_2|^4 \\ + \lambda_{\Phi H_2} |\Phi|^2 |H_2|^2 + \lambda_{\Phi H} |\Phi|^2 |H|^2. \end{aligned} \tag{2}$$

Here, v_D is the vacuum expectation value (VEV) of the singlet scalar $\Phi(\equiv \phi/\sqrt{2})$. In order to realize electroweak vacuum, the coupling $\lambda_{\Phi H}$ with the standard model (SM)

[2]Here, we remain agnostic about the origin of such an asymmetry. Example of a UV complete model can be found in [36]. The GW phenomenology discussed here is generic and independent of such UV completions.

Higgs H is suppressed. The one-loop correction to the tree-level potential is computed considering the couplings of all the particles to the singlet scalar Φ and this correction is known as Coleman-Weinberg (CW) potential [68], which can be written as

$$V_{\rm CW}(\phi) = \frac{1}{64\pi^2}\sum_{i=\phi,\phi',H_2,\chi} n_i M_i^4(\phi)\left\{\log\left(\frac{M_i^2(\phi)}{v^2}\right) - C_i\right\} \tag{3}$$

where, $n_\Phi = 1$, $n_{\Phi'} = 1$, $n_{H_2} = 4$ and $n_\chi = 2$ and $C_{\Phi,\Phi',H_2,\chi} = \frac{3}{2}$. The physical field-dependent masses of all particles are

$$M_\Phi^2(\phi) = \lambda_D(3\phi^2 - v_D^2), \qquad M_{\Phi'}^2(\phi) = m_{\Phi'}^2 + \frac{\lambda_{\Phi\Phi'}\phi^2}{2},$$
$$M_{H_2}^2(\phi) = m_{H_2}^2 + \frac{\lambda_{\Phi H_2}\phi^2}{2}, \qquad M_\chi^2(\phi) = (m_\chi + g_\chi\phi)^2.$$

Now, the thermal contributions to the effective potential [69,70] can be expressed as

$$V_T(\phi,T) = \sum_{i=\Phi,\Phi',H_2}\frac{n_i T^4}{2\pi^2}J_B\left(\frac{M_i^2(\phi)}{T^2}\right) - \frac{n_\chi T^4}{2\pi^2}J_F\left(\frac{M_\chi^2(\phi)}{T^2}\right) \tag{4}$$

where

$$J_F(x) = \int_0^\infty dy y^2 \log\left[1 + e^{-\sqrt{y^2+x^2}}\right],$$
$$J_B(x) = \int_0^\infty dy y^2 \log\left[1 - e^{-\sqrt{y^2+x^2}}\right].$$

Besides this, the Daisy corrections [71–73] are also incorporated in thermal contribution to improve perturbative expansion considering Arnold-Espinosa method [73] during FOPT such that $V_{\rm thermal}(\phi,T) = V_T(\phi,T) + V_{\rm daisy}(\phi,T)$. The Daisy contribution can be written as

$$V_{\rm daisy}(\phi,T) = -\frac{T}{2\pi^2}\sum_{i=\Phi',H_2} n_i[M_i^3(\phi,T) - M_i^3(\phi)] \tag{5}$$

where, $M_i^2(\phi,T) = M_i^2(\phi) + \Pi_i(T)$ and the relevant thermal masses are

$$M_{\Phi'}^2(\phi,T) = m_{\Phi'}^2(\phi) + \left(\frac{\lambda_{\Phi'}}{4} + \frac{\lambda_{\Phi\Phi'}}{6}\right)T^2,$$
$$M_{H_2}^2(\phi,T) = m_{H_2}^2(\phi) + \left(\frac{\lambda_{H_2}}{4} + \frac{\lambda_{\Phi H_2}}{12}\right)T^2.$$

So, at finite temperature, the effective potential can be written as

$$V_{\rm eff}(\phi,T) = V_{\rm tree}(\phi) + V_{\rm CW}(\phi) + V_{\rm thermal}(\phi,T). \tag{6}$$

At high temperatures, the Universe lies in a vacuum $\langle\phi\rangle = 0$. When the temperature decreases to a critical temperature T_c, two degenerate vacua are created which are separated by a barrier. Below this critical temperature, the Universe tunnels through the barrier from false vacuum $\langle\phi\rangle = 0$ to true vacuum $\langle\phi\rangle \neq 0$. The rate of tunneling is estimated by calculating the bounce solution [74]. The tunneling rate per unit volume is defined in terms of O(3) symmetric bounce action $S_3(T)$ as

$$\Gamma(T) \sim T^4 e^{-S_3(T)/T}. \tag{7}$$

The nucleation temperature T_n is calculated by comparing the tunneling rate with the Hubble expansion rate as

$$\Gamma(T_n) = \mathbf{H}^4(T_n) = \mathbf{H}_*^4. \tag{8}$$

The volume fraction of false vacuum of the Universe is defined by $p(T) = e^{-\mathcal{I}(T)}$ [75,76], where

$$\mathcal{I}(T) = \frac{4\pi}{3}\int_T^{T_c}\frac{dT'}{T'^4}\frac{\Gamma(T')}{\mathbf{H}(T')}\left(\int_T^{T'}\frac{d\tilde{T}}{\mathbf{H}(\tilde{T})}\right)^3. \tag{9}$$

The percolation temperature T_p is then calculated by using $\mathcal{I}(T_p) = 0.34$ [75] indicating that at least 34% of the comoving volume is occupied by the true vacuum. After the nucleation, an amount of energy is released as latent heat related to the change of energy-momentum tensor across the bubble wall during the FOPT [77,78] given by

$$\alpha_* = \frac{\epsilon}{\rho_{\rm rad}} \tag{10}$$

where, $\epsilon = (\Delta V_{\rm eff} - \frac{T}{4}\frac{\partial\Delta V_{\rm eff}}{\partial T})_{T=T_n}$, $\Delta V_{\rm eff} = V_{\rm eff}(\phi_{\rm false},T) - V_{\rm eff}(\phi_{\rm true},T)$ and $\rho_{\rm rad} = g_*\pi^2T^4/30$. Here, g_* denotes the total relativistic degrees of freedom. The time span of FOPT is denoted by the parameter $\beta/\mathbf{H}(T) \simeq T\frac{d}{dT}(\frac{S_3}{T})$, whereas, the bubble wall velocity v_w, in general, is related to the Jouguet velocity $v_J = \frac{1/\sqrt{3}+\sqrt{\alpha_*^2+2\alpha_*/3}}{1+\alpha_*}$. For the type of FOPT we are considering, $v_w \approx v_J$ [79–81] whereas in the presence of supercooling they are related nontrivially [82]. In these analyses, the calculation for the action $S_3(T)$ can be performed numerically by fitting the effective potential given by Eq. (6) to a generic potential [83]. The details of this procedure is described in Ref. [84].

III. PBH FORMATION FROM FERMI-BALL

As the FOPT proceeds, the true vacuum expands to cover the whole Universe, while the false vacuum gradually shrinks to a smaller region. At a later stage, the false vacuum region contracted into smaller disconnected

volumes, which again split to negligible size at percolation temperature [75]. Within these final pockets of false vacuum, some preexisting asymmetry of χ fermions can get trapped and the symmetric part annihilates via $\chi\chi \to \mathrm{S}$ and $\chi\chi \to \mathrm{SS}$, to final state particles S (either SM particles or ϕ) through decay or annihilation. Now, the trapped χ's create a degeneracy pressure. If such a pressure is able to balance the vacuum pressure, these χ remnants form a bound state which is known as Fermi-ball [35,85–87]. These Fermi-balls formed at T_* defined by $p(T_*) = 0.29$. The energy of a Fermi-ball can be written as

$$E_{\rm FB} = \frac{3\pi}{4}\left(\frac{3}{2\pi}\right)^{2/3}\frac{Q_{\rm FB}^{4/3}}{R} + \frac{4\pi}{3}U_0(T_*)R_{\rm FB}^3, \quad (11)$$

where, $Q_{\rm FB} = F_\chi^{\rm trap}\frac{n_\chi - n_{\bar\chi}}{n_{\rm FB}^*}$ with n_X denoting number density of X, $F_\chi^{\rm trap} \approx 1$ for maximum trapping of χ inside false vacuum and U_0 is vacuum energy. Now, minimizing the Fermi-ball energy, we can get the mass and radius as

$$M_{\rm FB} = Q_{\rm FB}(12\pi^2 U_0(T_*))^{1/4}, \quad R_{\rm FB}^3 = \frac{3}{16\pi}\frac{M_{\rm FB}}{U_0(T_*)}. \quad (12)$$

Within the Fermi-balls, the χ's interact through attractive Yukawa interaction $g_\chi\phi\bar\chi\chi$ and the interaction range is $L_\phi(T) = (\frac{d^2V_{\rm eff}}{d\phi^2}|_{\phi=0})^{-1/2}$ [64]. The Yukawa potential energy contribution to the Fermi-ball energy can be expressed as

$$E_Y \simeq -\frac{3g_\chi^2}{8\pi}\frac{Q_{\rm FB}^2}{R_{\rm FB}}\left(\frac{L_\phi}{R_{\rm FB}}\right)^2. \quad (13)$$

At a later stage, when the Yukawa potential energy becomes larger than the Fermi-ball energy, the Fermi-ball becomes unstable and collapses to form PBH [35]. We consider that the Fermi-ball formation temperature is close to the nucleation temperature, $T_* \sim T_n$. The initial PBH mass during formation can be estimated in terms of FOPT parameters as [35]

$$M_{\rm in} \sim 1.4\times 10^{21}\times v_w^3\left(\frac{\eta_\chi}{10^{-3}}\right)\left(\frac{100}{g_*}\right)^{1/4} \times \left(\frac{100\ \text{GeV}}{T_*}\right)^2\left(\frac{100}{\beta/\mathbf{H}_*}\right)^3\alpha_*^{1/4}\ \text{g}. \quad (14)$$

The initial temperature of the black hole is related to its mass as $T_{\rm BH}^{\rm in} \simeq 10^{13}\ \text{GeV}(\frac{1\ \text{g}}{M_{\rm in}})$. The initial abundance of PBH which is characterized by the parameter $\beta_{\rm PBH}$, defined as the ratio of the energy density of PBH to the total energy density, is obtained to be [35]

$$\beta_{\rm PBH} \sim 1.4\times 10^{-15}\times v_w^{-3}\left(\frac{g_*}{100}\right)^{1/2}\left(\frac{T_*}{100\ \text{GeV}}\right)^3 \times \left(\frac{\beta/\mathbf{H}_*}{100}\right)^3\left(\frac{M_{\rm in}}{10^{15}\ \text{g}}\right)^{3/2}. \quad (15)$$

Now, if the initial abundance of PBH is large enough, PBH can dominate the energy density of the Universe over radiation. This puts a lower bound on $\beta_{\rm PBH}$ for PBH domination, given by

$$\beta_{\rm PBH} \gtrsim \beta_{\rm crit} \simeq \frac{T_{\rm evap}}{T_n}, \quad (16)$$

where $T_{\rm evap} \simeq (\frac{9g_*(T_{\rm BH}^{\rm in})}{10240})^{\frac{1}{4}}(\frac{M_{\rm P}^5}{M_{\rm in}^3})^{\frac{1}{2}}$ indicates the temperature of the thermal bath when PBH evaporates. Solving Eq. (14) and (15), we can connect the FOPT parameters T_n and $\beta/\mathbf{H}_*$ to the PBH parameters $M_{\rm in}$ and $\beta_{\rm PBH}$ as

$$T_n = 1.61\times 10^{18}\beta_{\rm PBH}\left(\frac{100}{g_*}\right)^{1/4}\left(\frac{M_{\rm in}}{1\ \text{g}}\right)^{-1/2} \times \left(\frac{\eta_\chi}{10^{-3}}\right)^{-1}\frac{1}{\alpha_*^{1/4}}\ \text{GeV}, \quad (17)$$

$$\beta/\mathbf{H}_* = 1.75\times 10^{-2}\alpha_*^{1/4}\left(\frac{\eta_\chi}{10^{-3}}\right)v_w\left(\frac{g_*}{100}\right)^{1/12}\beta_{\rm PBH}^{-2/3}. \quad (18)$$

It should be noted that, we require to maintain $g_\chi v_D > T_n$ to ensure that the fermion χ's get trapped inside the false vacuum and its penetration to the true vacua is kinematically disfavored.

IV. GW FROM FOPT

The stochastic GW spectrum from a FOPT can be estimated by considering all the relevant contributions from bubble collisions [88–92], the sound wave [93–96] and the turbulence [79,97–101] of the plasma medium. So, the stochastic GW spectrum can be written as [102]

$$\Omega_{\rm GW}^{\rm PT}(f) = \Omega_\phi(f) + \Omega_{\rm sw}(f) + \Omega_{\rm turb}(f), \quad (19)$$

where $\Omega_\phi, \Omega_{\rm sw}, \Omega_{\rm turb}$ are individual contributions from bubble collisions, sound wave of the plasma and turbulence in the plasma respectively. The GW spectrum for bubble collision can be written as [102]

$$\Omega_\phi h^2 = 1.67\times 10^{-5}\left(\frac{100}{g_*}\right)^{1/3}\left(\frac{\mathbf{H}_*}{\beta}\right)^2\left(\frac{\kappa\alpha_*}{1+\alpha_*}\right)^2 \times \frac{0.11v_w^3}{0.42+v_w^2}\frac{3.8\left(f/f_{\rm peak}^{{\rm PT},\phi}\right)^{2.8}}{1+2.8\left(f/f_{\rm peak}^{{\rm PT},\phi}\right)^{3.8}}, \quad (20)$$

with the peak frequency [102] given by

$$f_{\rm peak}^{{\rm PT},\phi} = 1.65\times10^{-5}\ {\rm Hz}\left(\frac{g_*}{100}\right)^{1/6}\left(\frac{T_n}{100\ {\rm GeV}}\right) \times \frac{0.62}{1.8-0.1v_w+v_w^2}\left(\frac{\beta}{\mathbf{H}_*}\right). \tag{21}$$

The efficiency factor κ_ϕ for bubble collision can be expressed as [79]

$$\kappa_\phi = \frac{1}{1+0.715\alpha_*}\left(0.715\alpha_* + \frac{4}{27}\sqrt{3\alpha_*/2}\right). \tag{22}$$

The GW spectrum produced from the sound wave in the plasma can be written as [77,102,103]

$$\Omega_{\rm sw}h^2 = 2.65\times10^{-6}\left(\frac{100}{g_*}\right)^{1/3}\left(\frac{\mathbf{H}_*}{\beta}\right)\left(\frac{\kappa_{\rm sw}\alpha_*}{1+\alpha_*}\right)^2 \times v_w\left(f/f_{\rm peak}^{\rm PT,sw}\right)^3\left(\frac{7}{4+3\left(f/f_{\rm peak}^{\rm PT,sw}\right)^2}\right)^{7/2}\Upsilon \tag{23}$$

and the corresponding peak frequency is given by [102]

$$f_{\rm peak}^{\rm PT,sw} = 1.65\times10^{-5}\ {\rm Hz}\left(\frac{g_*}{100}\right)^{1/6}\left(\frac{T_n}{100\ {\rm GeV}}\right)\left(\frac{\beta}{H_*}\right)\frac{2}{\sqrt{3}}. \tag{24}$$

The efficiency factor for sound wave can be expressed as [81]

$$\kappa_{\rm sw} = \frac{\sqrt{\alpha_*}}{0.135+\sqrt{0.98+\alpha_*}}. \tag{25}$$

The suppression factor $\Upsilon = 1-\frac{1}{\sqrt{1+2\tau_{sw}H_*}}$ depends on the lifetime of sound wave $\tau_{\rm sw}$ [103] given by $\tau_{\rm sw}\sim R_*/\bar{U}_f$ where mean bubble separation is $R_* = (8\pi)^{1/3}v_w\beta$ and rms fluid velocity is $\bar{U}_f = \sqrt{3\kappa_{sw}\alpha_*/4}$.

Finally, the GW spectrum generated by the turbulence in the plasma is given by [102]

$$\Omega_{\rm turb}h^2 = 3.35\times10^{-4}\left(\frac{100}{g_*}\right)^{1/3}\left(\frac{\mathbf{H}_*}{\beta}\right)\left(\frac{\kappa_{\rm turb}\alpha_*}{1+\alpha_*}\right)^{3/2}v_w \times \frac{\left(f/f_{\rm peak}^{\rm PT,turb}\right)^3}{\left(1+f/f_{\rm peak}^{\rm PT,turb}\right)^{11/3}(1+8\pi f/h_*)} \tag{26}$$

with the peak frequency as [102]

$$f_{\rm peak}^{\rm PT,turb} = 1.65\times10^{-5}\ {\rm Hz}\left(\frac{g_*}{100}\right)^{1/6}\left(\frac{T_n}{100\,{\rm GeV}}\right)\frac{3.5}{2}\left(\frac{\beta}{H_*}\right). \tag{27}$$

The efficiency factor for turbulence is $\kappa_{\rm turb}\simeq0.1\kappa_{\rm sw}$ and the inverse Hubble time at the epoch of GW emission, redshifted to today is

$$h_* = 1.65\times10^{-5}\frac{T_n}{100\ {\rm GeV}}\left(\frac{g_*}{100}\right)^{1/6}. \tag{28}$$

It is clear from the above expressions that the contribution from sound waves turns out to be the most dominant one and the peak of the total GW spectrum corresponds to the peak frequency of sound waves contribution.

V. GW FROM PBH DENSITY FLUCTUATIONS

While there are several ways in which PBH can give rise to GW [45–47,104], for our purpose of ultralight PBH, the GW spectrum generated by most of these mechanisms lies at very high frequencies. Hence, we rather focus on GW generated because of the inhomogeneity in the PBH distribution after they are formed [49–51,105,106]. Such a spectrum is independent of the formation mechanism of PBH, and is within reach of near-future GW detectors.

After PBH are formed, they are inhomogeneously distributed in space following Poisson statistics [49]. These inhomogeneities can induce GW at second order once PBH dominates the energy density of the Universe [49,50], which gets further enhanced during PBH evaporation [50]. The dominant contribution to the GW spectrum observed today can be written as [21,50,51,107]

$$\Omega_{\rm GW}^{\rm PBH}\simeq\Omega_{\rm peak}^{\rm PBH}\left(\frac{f}{f_{\rm peak}^{\rm PBH}}\right)^{11/3}\Theta\left(f_{\rm peak}^{\rm PBH}-f\right). \tag{29}$$

Note that there exists an ultraviolet cutoff that corresponds to length scales smaller than the mean separation between PBH, below which the PBH cannot be treated as a continuous fluid. The associated frequency is estimated to be

$$f_{\rm peak}^{\rm PBH}\simeq1.7\times10^3\ {\rm Hz}\left(\frac{M_{\rm in}}{10^4\ {\rm g}}\right)^{-5/6}. \tag{30}$$

The peak amplitude, on the other hand, is given by

$$\Omega_{\rm peak}^{\rm PBH}\simeq9.67\times10^{-11}\left(\frac{k_{\rm UV}}{k_{\rm eva}}\right)^{17/3}\left(\frac{k_{\rm eq}}{k_{\rm UV}}\right)^8, \tag{31}$$

where $k_{\rm UV}$ corresponds to the comoving wave number corresponding to the mean separation between PBH, whereas $k_{\rm eq}$, $k_{\rm eva}$ indicates the comoving wave number of the modes entering the horizon when PBH begins to

dominate and when they evaporate respectively. The ratio of the comoving wave numbers are found using [50] $k_{\rm UV}/k_* = (\frac{3M_{\rm in}}{4\pi\rho^{\rm in}_{\rm PBH}})^{-1/3}\mathbf{H}_*^{-1}$, $k_{\rm eq}/k_* = \sqrt{2}\beta^{2/3}_{\rm PBH}$ and $k_{\rm eva}/k_* = (\beta_{\rm PBH}H_{\rm eva}/\mathbf{H}_*)^{1/3}$, where $\rho^{\rm in}_{\rm PBH}$, k_* and $H_{\rm eva}$ (H_*) denotes the initial energy density of PBH, wavenumber at the time of PBH formation, Hubble parameter at the time of PBH evaporation (formation) respectively. Expressing explicitly in terms of the PBH formation temperature $T_* \simeq T_n$, we get

$$\frac{k_{\rm UV}}{k_{\rm eva}} \simeq 10^6 \left(\frac{M_{\rm in}}{10^4\ {\rm g}}\right)^{2/3}, \tag{32}$$

$$\frac{k_{\rm eq}}{k_{\rm UV}} \simeq 3.18\times 10^{-11}(\beta_{\rm PBH})^{2/3}\left(\frac{M_{\rm in}}{1\ {\rm g}}\right)^{1/3}\left(\frac{T_n}{1\ {\rm GeV}}\right)^{2/3}. \tag{33}$$

Using the above ratio of wave numbers in Eq. (31), we can write the GW amplitude as

$$\Omega^{\rm PBH}_{\rm peak} \simeq 4.75\times 10^{-20}(\beta_{\rm PBH})^{16/3}\left(\frac{M_{\rm in}}{10^7\ {\rm g}}\right)^{58/9}\left(\frac{T_n}{100\,{\rm GeV}}\right)^{16/3}. \tag{34}$$

Note that for PBH formed through Fermi-ball collapse, T_n in turn depends on the PBH parameters and the asymmetry η_χ through Eq. (17).

Now, since GW behave as radiation, they can contribute to extra relativistic degrees of freedom during the epoch of BBN. GW from PBH density fluctuations can violate the BBN bound from Planck, if the GW amplitude is very large. This translates into an upper bound on the initial PBH fraction $\beta_{\rm PBH}$, which we find to be given by

$$\beta_{\rm PBH} \lesssim \beta_{\rm max} \simeq 1.8\times 10^{-4}\left(\frac{M_{\rm in}}{10^4\ {\rm g}}\right)^{-17/32}\left(\frac{\alpha}{0.1}\right)^{3/16}\left(\frac{\beta/\mathbf{H}_*}{10}\right)^{3/4}. \tag{35}$$

VI. THE COMBINED SPECTRA AND DETECTION PROSPECTS

If PBH are formed during the phase transition through Fermi-ball collapse, they can leave their indirect imprints in the GW spectrum. Considering the dominant sound wave contribution and using Eq. (17) and (18), we can analytically relate the FOPT GW spectrum to the PBH mass and initial abundance approximately as

$$f^{\rm PT}_{\rm peak} \simeq \frac{5.33\times 10^9}{S^{1/3}}\beta^{1/3}_{\rm PBH}\left(\frac{M_{\rm in}}{1\ {\rm g}}\right)^{-1/2}\ {\rm Hz}, \tag{36}$$

$$\Omega^{\rm PT}_{\rm peak}h^2 \simeq \frac{1.42\times 10^{-7}}{S^{4/3}}\beta^{2/3}_{\rm PBH}\alpha_*^{-1/4}\eta_\chi^{-1}\left(\frac{\kappa_{\rm sw}\alpha_*}{1+\alpha_*}\right)^2. \tag{37}$$

Here, the factor S accounts for the extra entropy dilution after the gravitational waves from FOPT are produced, which is because of PBH domination and their subsequent evaporation. This makes the frequency and the FOPT generated GW amplitude more redshifted, compared to the usual scenario without PBH domination. The factor S can be approximated as

$$S \simeq \frac{T_{\rm dom}}{T_{\rm eva}} = \beta\frac{T_n}{T_{\rm eva}}, \tag{38}$$

where $T_{\rm dom}$ indicates the temperature of the Universe when PBH starts to dominate. Now, note that the peak frequency depends explicitly both on the PBH mass as well as the initial abundance of PBH, but not on the asymmetry η_χ. On the other hand, the peak amplitude is not dependent on the PBH mass explicitly, but is sensitive to the initial abundance of PBH as well as the asymmetry η_χ.

Considering the contribution of GW from PBH density perturbations, the combined spectrum exhibits a unique doubly peaked feature. While the peak at the higher frequency corresponds to the contribution from FOPT, the sharp peak at the lower frequency is the contribution from PBH density fluctuations. In Fig. 1, we show the combined GW spectrum varying the initial PBH mass $M_{\rm in}$ (left panel) and initial PBH abundance $\beta_{\rm PBH}$ for a fixed PBH mass (right panel). Note that changing $M_{\rm in}$ also changes $\beta_{\rm PBH}$ in the left panel [cf. Eq. (15)]. The other details of these benchmark points are given in Table I. In all these plots, the experimental sensitivities of SKA [108], GAIA [109], THEIA [109], μARES [110], LISA [111], AEDGE [112], DECIGO [58], UDECIGO (UDECIGO-corr) [62,63], BBO [59], ET [60], CE [61] and aLIGO (HL) [113] are shown as shaded regions of different colors. The horizontal dashed red-colored line corresponds to the BBN limit on effective relativistic degrees of freedom from GW.

The value of the initial asymmetry η_χ depends on the details of the χ dynamics in the early Universe before the phase transition, and is generally unconstrained. However, the constraints on the PBH abundance $\beta_{\rm PBH}$ can constrain η_χ, since for PBH formation from Fermi-ball collapse, η_χ is related to $\beta_{\rm PBH}$ through Eq. (17) and (18). In Fig. 2, we show the allowed η_χ values in the $M_{\rm PBH} - \eta_\chi$ plane, along with corresponding values of the temperature T_n in color code for two different values of $\beta/\mathbf{H}_*$. The gray shaded upper triangular region is ruled out since here $\beta_{\rm PBH} > \beta_{\rm max}$, leading to overproduction of GW violating BBN bounds, as discussed earlier. On the other hand, in the gray shaded lower triangular region, $\beta_{\rm PBH}$ turns out to be less than $\beta_{\rm crit}$, which does not lead to PBH domination. In such a case, GW from density fluctuations do not exist, leading to only a single peak feature in the GW spectra, arising from the phase transition. The double peak feature is also absent if the peak of GW contribution from PBH density fluctuation falls below the corresponding GW amplitude from FOPT,

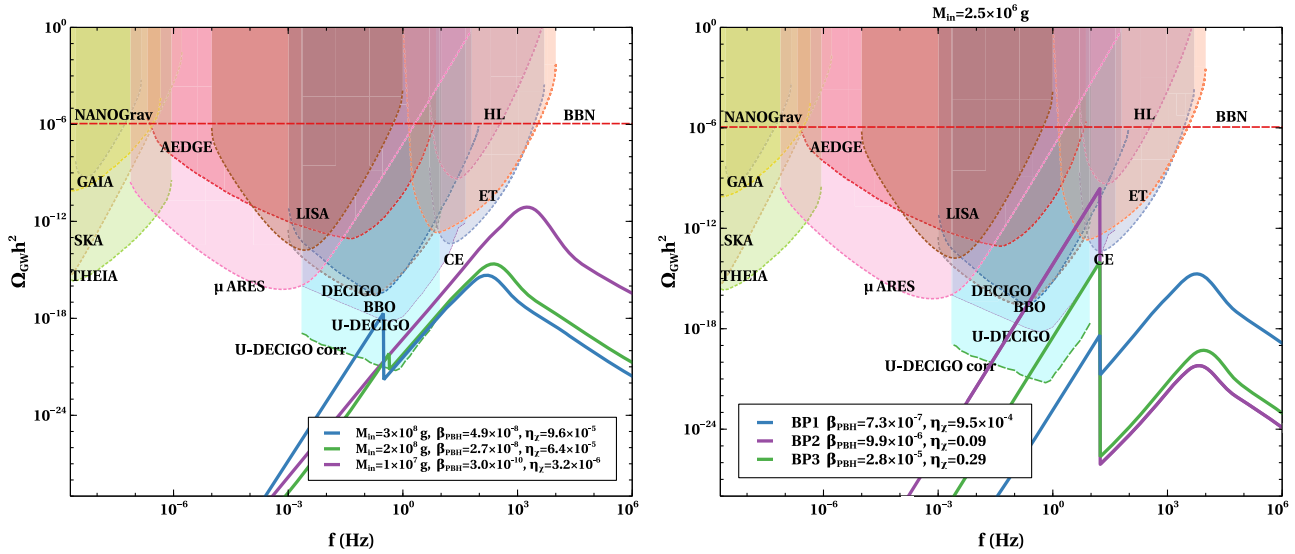

FIG. 1. Combined GW spectrum from phase transition and PBH density fluctuations for BP4 (see Table I), considering different values of $M_{\rm in}$ (left panel), and for BP1, BP2 and BP3 for a fixed $M_{\rm in}$ (right panel) but different values of $\beta_{\rm PBH}$.

i.e., $\Omega^{\rm PBH}_{\rm peak} < \Omega^{\rm PT}_{\rm GW}(f^{\rm PBH}_{\rm peak})$. As the GW peak arising from the FOPT remains outside the sensitivities of low frequency experiments for most part of the parameter space, we show the parameter space and sensitivities to the GW peak arising from PBH density perturbations in Fig. 3. However, for subdominant PBH, the GW peak from FOPT does not suffer any entropy dilution and can be brought within sensitivities of several experiments which we discuss below along with the corresponding implications for DM phenomenology.

VII. IMPLICATIONS FOR DM PHENOMENOLOGY

As seen in the previous section, if PBH dominates the energy density of the Universe we observe a unique doubly-peaked spectrum. However, the second peak at the higher frequency sourced by the FOPT remains out of reach of future GW experiments like ET, CE, DECIGO, BBO. This is primarily because of the extra redshift and dilution arising because of PBH domination and subsequent evaporation [cf. Eq. (36), (37)]. If PBH do not dominate the energy density, the single peak can be within reach of future GW sensitivity. This can also have interesting consequences in terms of producing the observed DM relic abundance, which otherwise is overproduced in the case of PBH domination, unless superheavy [20,114].

The dark sector fermion χ in our setup cannot lead to the observed DM abundance, because of being trapped in the false vacuum. However χ can still be produced from PBH evaporation [41,42] or from the SM bath. Also, some small fraction of χ can cross from the false vacuum to the true vacuum [115]. While a detailed calculation of such trapping and crossing is beyond the scope of our present work, simple conservative estimates, shown in Appendix justifies maximum trapping. In all such cases where χ appears in the true vacuum, the interaction of χ with the SM bath can play crucial role in deciding its final relic. Since we remain agnostic about the UV completion of the dark sector, we do not consider the possibility of χ being DM. The amount of χ produced from the above possible ways can finally decay into the SM bath, before the BBN epoch. As long as χ is long-lived enough and decay at a temperature $T_{\rm decay} \ll T_*$, the formation temperature of PBH, the phenomenology discussed here remain unaffected. Such a decay of χ can be introduced via explicit $U(1)_D$ global symmetry breaking higher dimensional operators like $\bar{\ell}_L \tilde{H} \chi \Phi/\Lambda$ where ℓ_L denotes the lepton doublet of the SM. Since χ is lighter in the false vacuum, depending upon the UV completion of

TABLE I. Benchmark parameters considered in the analysis.

	v_D (GeV)	g_χ	$\lambda_{\Phi\Phi'}$	$\lambda_{\Phi H_2}$	T_c (GeV)	T_n (GeV)	T_p (GeV)	T_* (GeV)	β/H_*	α_*	v_J
BP1	10^{10}	1.4	1.8	2.5	2.8×10^9	1.6×10^9	1.3×10^9	1.3×10^9	95	0.12	0.78
BP2	2×10^9	1.5	1.9	2.3	3.3×10^8	2.6×10^8	2.6×10^8	2.6×10^8	1014	0.03	0.70
BP3	10^9	1.4	1.8	2.3	2.9×10^8	2.3×10^8	2.2×10^8	2.2×10^8	1729	0.04	0.71
BP4	10^9	1.4	1.8	2.5	2.1×10^8	1.2×10^8	7.9×10^7	7.9×10^7	58	0.12	0.78

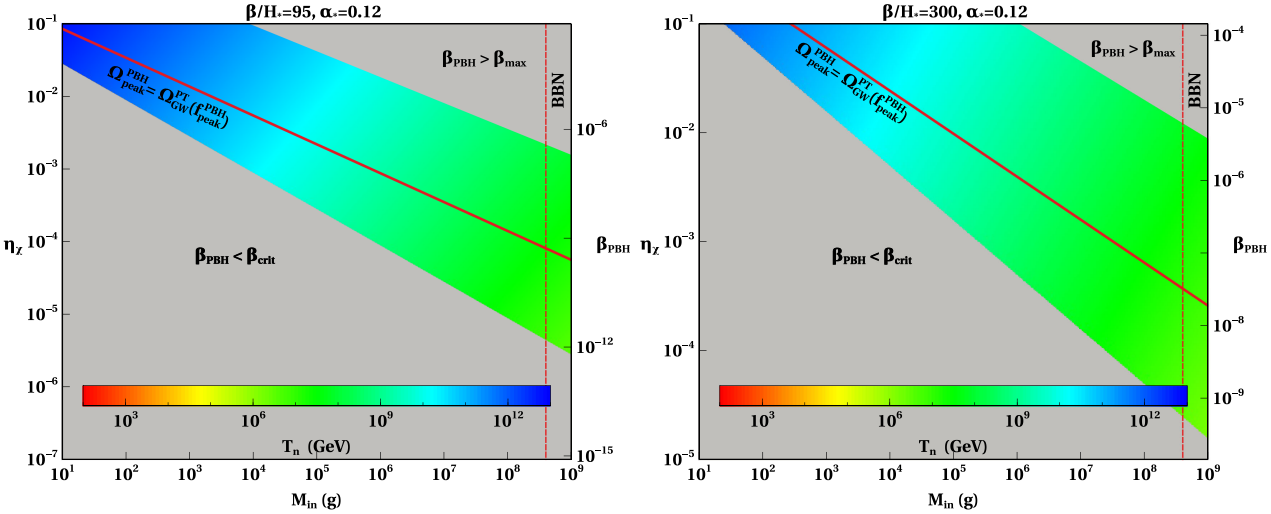

FIG. 2. $M_{\rm in} - \eta_\chi$ parameter space with $\beta/\mathbf{H}_* = 95$, $\alpha_* = 0.12$ (left panel) and $\beta/H_* = 300$, $\alpha_* = 0.12$ (right panel).

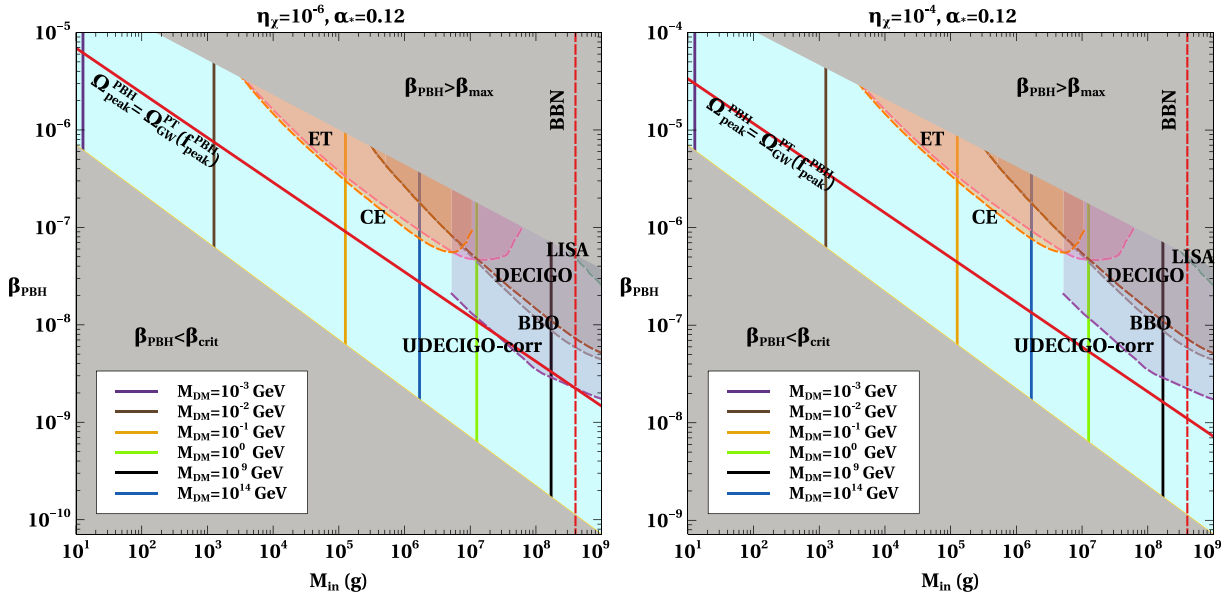

FIG. 3. $M_{\rm in} - \beta_{\rm PBH}$ parameter space for $\eta_\chi = 10^{-6}$, $\alpha_* = 0.12$ (left panel) and $\eta_\chi = 10^{-4}$, $\alpha_* = 0.12$ (right panel) showing the sensitivity of different experiments to the GW peak from PBH density perturbations.

the dark sector, it is also possible to ensure DM decay in the true vacuum while preventing the same in the false vacuum due to kinematical restrictions.

If we consider the dark sector to be purely gravitational in agreement with all experimental evidences, it can still be produced from PBH evaporation since the process of Hawking radiation is based solely on gravitational interactions.[3] For the case of subdominant PBH ($\beta < \beta_{\rm crit}$), the DM relic density produced from PBH evaporation is found to be[4] [8,18,117,118]

$$\Omega_{\rm DM}h^2 \simeq M_{\rm DM}\beta_{\rm PBH}\frac{T_n}{M_{\rm in}}\begin{cases}\left(\frac{M_{\rm in}}{M_P}\right)^2 & \text{for } M_{\rm DM} < T_{\rm BH}^{\rm in},\\ \left(\frac{M_P}{M_{\rm DM}}\right)^2 & \text{for } M_{\rm DM} > T_{\rm BH}^{\rm in},\end{cases} \tag{39}$$

[3]PBHs can also leave Planck remnants after evaporation, which can act as DM and have their imprints on GW. See Ref. [116].

[4]Here, for our demonstration, we consider the dark sector to consist of scalar particles. Similar results can be obtained for other particles depending on their degrees of freedom.

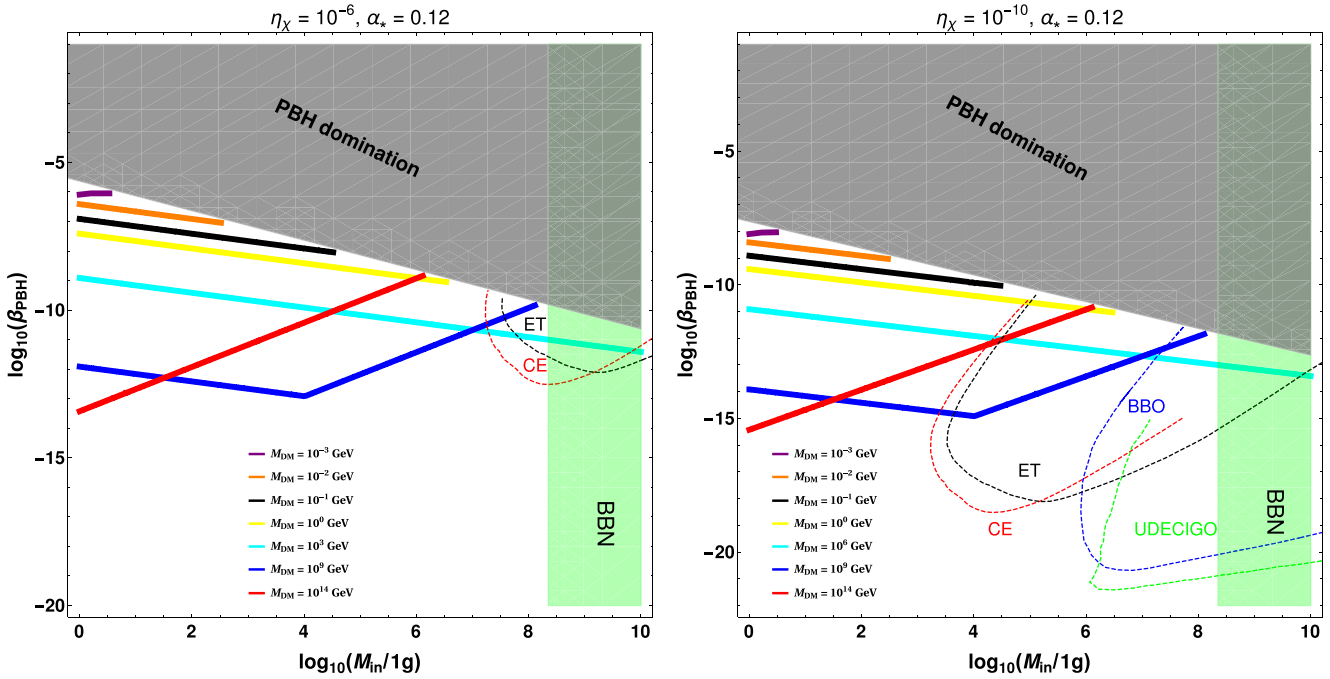

FIG. 4. Contours satisfying the observed DM relic abundance for different values of DM mass, considering $\eta_\chi = 10^{-6}$ (left panel) and $\eta_\chi = 10^{-10}$ (right panel).

where $M_{\rm DM}$ indicates the DM mass. Note that T_n in turn, depends on the PBH mass and initial fraction [cf. Eq. (17)]. On the other hand, in the case of PBH domination, the DM relic density is given by

$$\Omega_{\rm DM}h^2 \simeq M_{\rm DM}\frac{T_{\rm ev}}{M_{\rm in}}\begin{cases}\left(\frac{M_{\rm in}}{M_P}\right)^2 & \text{for } M_{\rm DM} < T_{\rm BH}^{\rm in},\\ \left(\frac{M_P}{M_{\rm DM}}\right)^2 & \text{for } M_{\rm DM} > T_{\rm BH}^{\rm in}.\end{cases} \tag{40}$$

As mentioned above, for PBH domination, DM gets overproduced from PBH evaporation irrespective of their spins and only $M_{\rm DM} \gtrsim 10^9$ GeV can lead to right abundance for $M_{\rm in} \gtrsim 10^6$ g [16,20,114]. DM over-production can also be controlled by choosing sufficiently light DM mass, but it is likely to face constraints from structure formation.

In Fig. 4, we show the contours of observed DM abundance in the $M_{\rm in} - \beta_{\rm PBH}$ plane considering two different values of the initial asymmetry η_χ. As we can see, for PBH domination regime, the DM mass range gets restricted while for subdominant PBH scenario, a much wider DM mass range becomes viable. While the value of η_χ does not change the DM parameter space, the GW sensitivity changes as changing η_χ also amounts to changing the FOPT parameters in order to generate the PBH of same initial mass and energy fraction. Clearly, future GW experiments like CE, ET, BBO, UDECIGO can probe a sizeable part of the parameter space in PBH mass ranging from $\mathcal{O}(1000\ \text{g})$ as well as DM masses ranging from GeV to superheavy ballpark. The detectable GW spectrum in this low frequency regime is purely generated by the FOPT in this case which is also free from any entropy dilution due to PBH evaporation. Figure 5 shows the GW spectrum of a few such benchmark points, the details of which are given in Table II. Similarly, the PBH domination region also remains within GW experimental sensitivities as shown in Fig. 3. While DM is mostly in the superheavy ballpark for such a scenario, PBH mass

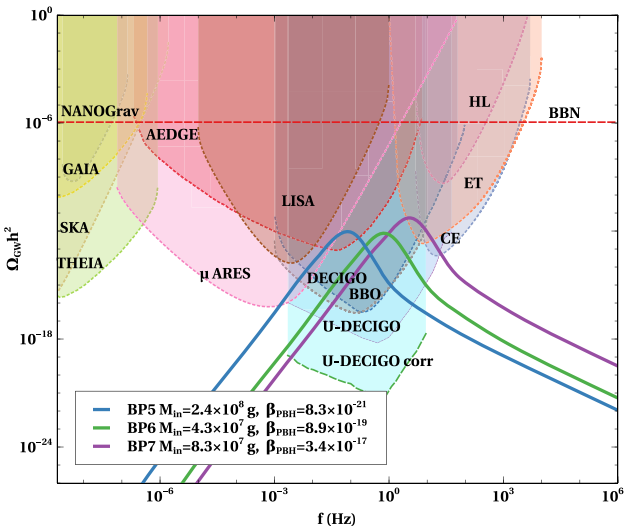

FIG. 5. GW spectrum from FOPT with subdominant PBH for different benchmark points.

TABLE II. Benchmark parameters considered in the analysis for subdominant PBH.

	v_D (GeV)	g_χ	$\lambda_{\Phi\Phi'}$	$\lambda_{\Phi H_2}$	T_c (GeV)	T_n (GeV)	T_p (GeV)	T_* (GeV)	β/H_*	α_*	v_J	η_χ
BP5	10^4	1.3	1.3	2.2	2.7×10^3	1.6×10^3	1.4×10^3	1.4×10^3	206	0.13	0.79	10^{-12}
BP6	10^5	1.4	1.3	2	3.2×10^4	2.1×10^4	1.8×10^4	1.7×10^4	140	0.09	0.76	10^{-11}
BP7	10^6	1.4	1.3	2.2	3.1×10^5	1.8×10^5	1.2×10^5	1.0×10^5	78	0.12	0.78	10^{-10}

$M_{\rm in} \gtrsim \mathcal{O}(1000\ {\rm g})$ can be probed by future GW experiments. While PBH mass range within GW sensitivities is similar in both the PBH dominance and subdominance cases, it is possible to distinguish these two scenarios at GW experiments due to different GW spectrum arising from PBH density fluctuations (PBH dominance) and FOPT (PBH subdominance).

Finally in Fig. 6, we show the contours of the observed DM relic density in $M_{\rm in} - M_{\rm DM}$ plane, for the two cases, i.e., PBH dominance (left panel) and subdominance (right panel). For a fixed PBH mass, the DM relic is satisfied at two DM mass values, either when DM is light ($M_{\rm DM} < T^{\rm in}_{\rm BH}$) or when DM is superheavy ($M_{\rm DM} > T^{\rm in}_{\rm BH}$) [cf. Eq. (39), (40)]. The free-streaming length of DM is constrained from Lyman-α flux-power spectra [119–121], which puts a constraint on light DM depending on the PBH mass [16,20,117,122]. This is due to the fact that light DM produced from such PBH evaporation can have relativistic speeds more than what is allowed for warm dark matter. This is shown by the gray-shaded region. For the PBH-dominance case, only the superheavy DM regime remains viable, while for subdominant PBH, we can satisfy the correct DM relic density at lighter DM mass as well while being consistent with Lyman-α bounds. The different colored contours along the relic density contour indicate the reach of future GW experiments that can probe the corresponding peak frequencies of the GW spectrum relevant for the PBH and DM mass. The left and the right panels specify the GW peak from density fluctuations and FOPT respectively, both having a one-to-one correspondence with the PBH mass [cf. Eq. (30), (36)], considering other parameters to be fixed.

VIII. PBH FROM OTHER MECHANISMS RELATED TO FOPT

Before concluding, we briefly comment on other FOPT origins of PBH and corresponding GW signatures. In other mechanisms without not relying on any dark sector asymmetry or Fermi ball collapse mechanism, PBH are formed when horizon-sized perturbations become more than the critical overdensity $\delta > \delta_c \sim 0.45$ leading to gravitational collapse [123]. Such type of gravitational collapse as a consequence of FOPT have been studied in

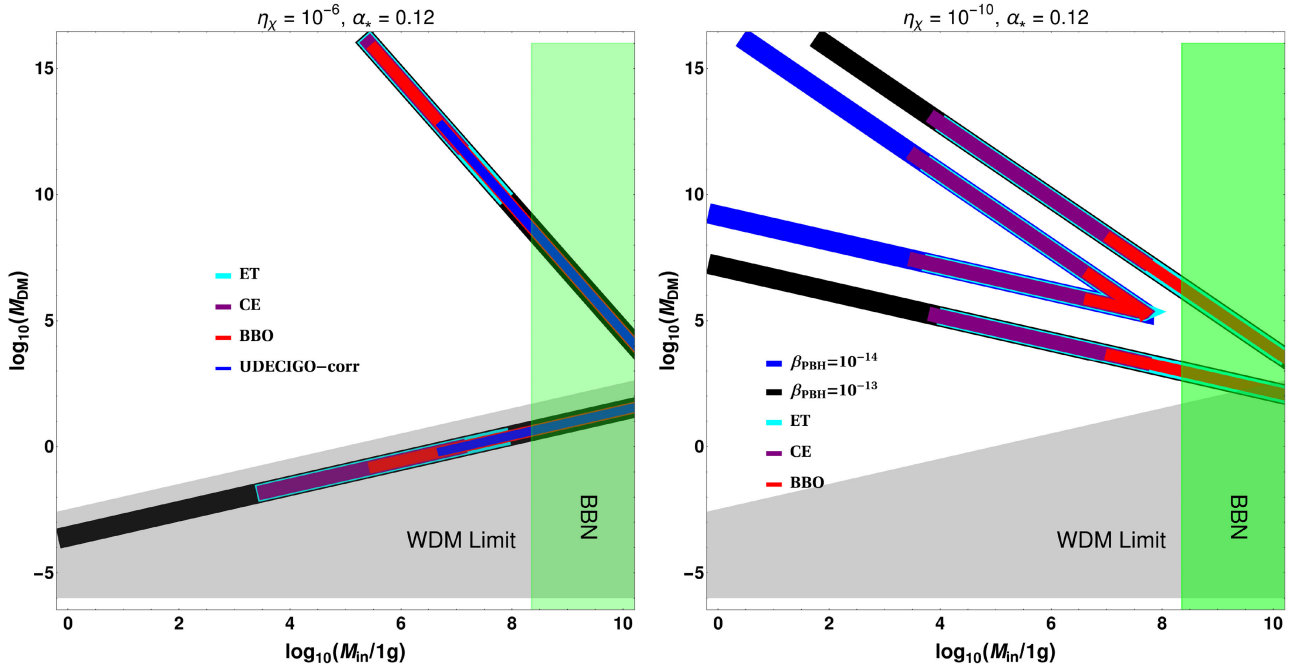

FIG. 6. Contours satisfying the observed DM relic abundance in $M_{\rm in} - M_{\rm DM}$ plane, considering $\eta_\chi = 10^{-6}$ with PBH domination (left panel) and $\eta_\chi = 10^{-10}$ with PBH subdomination (right panel), along with the future GW experiments that can probe our scenario. The gray-shaded region is constrained from warm dark matter bounds.

several works including [38,39,124,125] and references therein. During FOPT, nucleation may get delayed in some Hubble-sized region, and the late decay of the false vacuum increases the total energy density. In an expanding Universe, the radiation energy density keeps on decreasing, whereas in some regions the vacuum energy density remains constant. This leads to total energy density higher than the threshold overdensity and the mass inside such Hubble-sized region collapses to form PBH. After solving the Friedmann equation and radiation energy density evolution equations [38] in late false vacuum decay region and background region, we can estimate the time, $t_{\rm PBH}$ when PBH formed and the initial PBH mass can be written as $M_{\rm PBH} = \frac{4\pi}{3}\mathbf{H}^{-3}(t_{\rm PBH})\rho_c$, where ρ_c is critical energy density.[5] In such mechanisms, ultralight PBH of mass $\sim 8\times 10^8$ g can be formed from FOPT with nucleation temperature of order 10^{13} GeV. Thus, if PBH is subdominant, the GW peak from FOPT will be in the ultrahigh frequency regime $\sim 10^7$ Hz which is far outside the reach of near-future GW experiments.[6] For PBH domination, the GW peak from FOPT can get redshifted to a lower frequency (depending on $\beta_{\rm PBH}$) because of entropy dilution during PBH evaporation. For instance, considering the PBH mass mentioned above and taking $\beta_{\rm PBH} \sim \beta_{\rm max}$, we find the FOPT peak in the frequency range of order 10^4 Hz, with a very small amplitude ($\Omega^{\rm PT}_{\rm peak}h^2 \lesssim 10^{-25}$) because of the entropy dilution. Moreover, note that a detailed analysis requires calculating the energy fraction PBH $\beta_{\rm PBH}$ through the probability of late false vacuum decay [124]. Therefore, the PBH formation mechanism adopted in this work offers more detection prospects irrespective of whether PBH dominates or remains subdominant.

IX. CONCLUSION

We have studied the detection prospects of an ultralight primordial black hole formation mechanism in gravitational wave experiments and consequences for production of gravitational dark matter from such PBH evaporation. Considering the Fermi-ball collapse mechanism of PBH in the context of a first-order phase transition, we consider the combined GW spectrum arising from the FOPT as well as PBH density fluctuations with the latter requiring a PBH dominated phase. We show that such a PBH formation mechanism leads to a unique doubly peaked GW spectrum. While the GW spectrum generated from FOPT suffers from entropy dilution at later stages due to ultralight PBH evaporation, the blue-tilted part of its arm for certain region of parameter space can remain within experimental sensitivity. Combined detection of both the GW peaks require new experiments in kHz frequency ballpark having sufficient sensitivity. The PBH domination scenario mostly produces superheavy DM whereas the subdominant PBH can generate a much wider range of DM. While the doubly peaked feature in subdominant PBH scenario disappears due to absence of GW generated by PBH density fluctuations, the FOPT generated GW can be brought within sensitivities of future GW experiments like CE, ET, BBO, UDECIGO corresponding to DM mass in GeV to superheavy regime and PBH mass as low as a few kg. The PBH domination regime remains within sensitivities of such experiments for PBH mass as low as a few kg and DM masses mostly in the superheavy ballpark. Due to the strong connection between PBH parameters and FOPT parameters which in turn affect DM mass from relic abundance criteria, we have interesting correlations and complementarity among different observables which can be tested in near future.

[5]Similar relation is obtained for PBH formed through bubble collisions [126].

[6]There have been several proposed ideas to look for these ultrahigh frequency gravitational waves. See Ref. [127] for a review.

ACKNOWLEDGMENTS

The work of D. B. is supported by the Science and Engineering Research Board (SERB), Government of India grant No. MTR/2022/000575 and No. CRG/2022/000603. The work of S. J. D. was supported by IBS under the project code, IBS-R018-D1. S. J. D. would like to thank the support and hospitality of the Tata Institute of Fundamental Research (TIFR), Mumbai, where a portion of this project was carried out.

APPENDIX: PARTICLE TRAPPING IN FALSE VACUUM

Initially, all particles are in the false vacuum state. As the first order phase transition proceeds, particles gain mass in the true vacuum. The bubble of true vacuum expands and tries to capture the particles in the plasma. Due to the dynamical change of mass in the true vacuum, only sufficiently energetic particles are able to enter the bubble while conserving energy. Here, we show a simple quantitative analysis of particles getting trapped or reflected from bubble wall to false vacuum following the works of [41,128]. We can estimate the particle flux going to true vacuum in the bubble wall rest frame. The number of particles passing through the bubble wall along -z direction (considered for simplicity) per area ΔS in Δt time can be written as

$$\frac{\Delta N_{\rm in}}{\Delta S} = g_i \int \frac{d^3p}{(2\pi)^3} \int_{r_0}^{r_0 - \frac{p_z \Delta t}{p}} dr \mathcal{T}(p)\, \Theta(-p_z) f(p,x) \qquad \text{(A1)}$$

where, r_0 is bubble radius, $\Theta(-p_z)$ is ensuring particles going inside and $\mathcal{T}(p) = \Theta(-p_z - m_i)$ satisfied energy conservation inside bubble. Also, g_i is degrees of freedom of particle with mass m_i in true vacuum. Here, $f(p,x)$ is the distribution function of particles in false vacuum and it

will be Bose-Einstein (BE) or Fermi-Dirac (FD) distribution. The distribution can be approximated to be Maxwell-Boltzmann distribution as $f(p,x) = e^{-\tilde{\gamma}(p+\tilde{v}p_z)/T}$, where $\tilde{v}$ is the velocity of fluid or plasma with respect to bubble wall and $\tilde{\gamma}$ is corresponding Lorentz factor. The flux of particles in bubble wall frame can be calculated from above Eq. (A1) as

$$J_w = g_i T^3 \left(\frac{\tilde{\gamma}(1-\tilde{v})m_i/T + 1}{4\pi^2\tilde{\gamma}^3(1-\tilde{v})^2}\right) e^{-\frac{\tilde{\gamma}(1-\tilde{v})m_i}{T}}. \quad \text{(A2)}$$

Since, the bubble is expanding with a wall velocity v_w, the average number density inside true vacuum in global plasma frame can be expressed as

$$n_{\text{in}} = \frac{J_w}{\gamma_w v_w}. \quad \text{(A3)}$$

So, the fraction of particle which gets trapped in false vacuum can be written as

$$F^{\text{trap}} = 1 - \frac{n_{\text{in}}}{n_{\text{eq}}} \quad \text{(A4)}$$

where, n_{eq} is equilibrium number density of particles. In general, the velocity of fluid or plasma $\tilde{v}$ depends on fluid dynamics. From Eq. (A4), it can be seen that F^{trap} is maximum ($\sim$1) for fluid velocity $\tilde{v}$ O(0.1).

[1] Y. B. Zel'dovich and I. D. Novikov, The hypothesis of cores retarded during expansion and the hot cosmological model, Sov. Astron. AJ (Engl. Transl.) **10**, 602 (1967).
[2] S. W. Hawking, Black hole explosions, Nature (London) **248**, 30 (1974).
[3] S. W. Hawking, Particle creation by black holes, Commun. Math. Phys. **43**, 199 (1975); **46**, 206(E) (1976).
[4] G. F. Chapline, Cosmological effects of primordial black holes, Nature (London) **253**, 251 (1975).
[5] B. J. Carr, Some cosmological consequences of primordial black-hole evaporations, Astrophys. J. **206**, 8 (1976).
[6] B. Carr, K. Kohri, Y. Sendouda, and J. Yokoyama, Constraints on primordial black holes, Rep. Prog. Phys. **84**, 116902 (2021).
[7] P. Gondolo, P. Sandick, and B. Shams Es Haghi, Effects of primordial black holes on dark matter models, Phys. Rev. D **102**, 095018 (2020).
[8] N. Bernal and O. Zapata, Dark matter in the time of primordial black holes, J. Cosmol. Astropart. Phys. 03 (2021) 015.
[9] A. M. Green, Supersymmetry and primordial black hole abundance constraints, Phys. Rev. D **60**, 063516 (1999).
[10] M. Y. Khlopov, A. Barrau, and J. Grain, Gravitino production by primordial black hole evaporation and constraints on the inhomogeneity of the early universe, Classical Quantum Gravity **23**, 1875 (2006).
[11] D.-C. Dai, K. Freese, and D. Stojkovic, Constraints on dark matter particles charged under a hidden gauge group from primordial black holes, J. Cosmol. Astropart. Phys. 06 (2009) 023.
[12] R. Allahverdi, J. Dent, and J. Osinski, Nonthermal production of dark matter from primordial black holes, Phys. Rev. D **97**, 055013 (2018).
[13] O. Lennon, J. March-Russell, R. Petrossian-Byrne, and H. Tillim, Black hole genesis of dark matter, J. Cosmol. Astropart. Phys. 04 (2018) 009.
[14] D. Hooper, G. Krnjaic, and S. D. McDermott, Dark radiation and superheavy dark matter from black hole domination, J. High Energy Phys. 08 (2019) 001.
[15] P. Sandick, B. S. Es Haghi, and K. Sinha, Asymmetric reheating by primordial black holes, Phys. Rev. D **104**, 083523 (2021).
[16] T. Fujita, M. Kawasaki, K. Harigaya, and R. Matsuda, Baryon asymmetry, dark matter, and density perturbation from primordial black holes, Phys. Rev. D **89**, 103501 (2014).
[17] S. Datta, A. Ghosal, and R. Samanta, Baryogenesis from ultralight primordial black holes and strong gravitational waves from cosmic strings, J. Cosmol. Astropart. Phys. 08 (2021) 021.
[18] S. Jyoti Das, D. Mahanta, and D. Borah, Low scale leptogenesis and dark matter in the presence of primordial black holes, J. Cosmol. Astropart. Phys. 11 (2021) 019.
[19] B. Barman, D. Borah, S. J. Das, and R. Roshan, Non-thermal origin of asymmetric dark matter from inflaton and primordial black holes, J. Cosmol. Astropart. Phys. 03 (2022) 031.
[20] B. Barman, D. Borah, S. Das Jyoti, and R. Roshan, Cogenesis of baryon asymmetry and gravitational dark matter from primordial black holes, J. Cosmol. Astropart. Phys. 08 (2022) 068.
[21] B. Barman, D. Borah, S. Jyoti Das, and R. Roshan, Gravitational wave signatures of a PBH-generated baryon-dark matter coincidence, Phys. Rev. D **107**, 095002 (2023).
[22] A. Cheek, L. Heurtier, Y. F. Perez-Gonzalez, and J. Turner, Primordial black hole evaporation and dark matter production: I. Solely Hawking radiation, Phys. Rev. D **105**, 015022 (2022).
[23] A. Chaudhuri, B. Coleppa, and K. Loho, Dark matter production from two evaporating PBH distributions, Phys. Rev. D **108**, 035040 (2023).
[24] R. Roshan and G. White, Using gravitational waves to see the first second of the Universe, arXiv:2401.04388.

[25] S. Hawking, Gravitationally collapsed objects of very low mass, Mon. Not. R. Astron. Soc. **152**, 75 (1971).
[26] B. J. Carr and S. W. Hawking, Black holes in the early Universe, Mon. Not. R. Astron. Soc. **168**, 399 (1974).
[27] S. Wang, T. Terada, and K. Kohri, Prospective constraints on the primordial black hole abundance from the stochastic gravitational-wave backgrounds produced by coalescing events and curvature perturbations, Phys. Rev. D **99**, 103531 (2019); **101**, 069901(E) (2020).
[28] C. T. Byrnes and P. S. Cole, Lecture notes on inflation and primordial black holes, arXiv:2112.05716.
[29] M. Braglia, A. Linde, R. Kallosh, and F. Finelli, Hybrid α-attractors, primordial black holes and gravitational wave backgrounds, J. Cosmol. Astropart. Phys. 04 (2023) 033.
[30] M. Crawford and D. N. Schramm, Spontaneous generation of density perturbations in the early Universe, Nature (London) **298**, 538 (1982).
[31] S. W. Hawking, I. G. Moss, and J. M. Stewart, Bubble collisions in the very early Universe, Phys. Rev. D **26**, 2681 (1982).
[32] I. G. Moss, Singularity formation from colliding bubbles, Phys. Rev. D **50**, 676 (1994).
[33] H. Kodama, M. Sasaki, and K. Sato, Abundance of primordial holes produced by cosmological first order phase transition, Prog. Theor. Phys. **68**, 1979 (1982).
[34] M. J. Baker, M. Breitbach, J. Kopp, and L. Mittnacht, Primordial black holes from first-order cosmological phase transitions, arXiv:2105.07481.
[35] K. Kawana and K.-P. Xie, Primordial black holes from a cosmic phase transition: The collapse of Fermi-balls, Phys. Lett. B **824**, 136791 (2022).
[36] P. Huang and K.-P. Xie, Primordial black holes from an electroweak phase transition, Phys. Rev. D **105**, 115033 (2022).
[37] K. Hashino, S. Kanemura, and T. Takahashi, Primordial black holes as a probe of strongly first-order electroweak phase transition, Phys. Lett. B **833**, 137261 (2022).
[38] J. Liu, L. Bian, R.-G. Cai, Z.-K. Guo, and S.-J. Wang, Primordial black hole production during first-order phase transitions, Phys. Rev. D **105**, L021303 (2022).
[39] Y. Gouttenoire and T. Volansky, Primordial black holes from supercooled phase transitions, arXiv:2305.04942.
[40] M. Lewicki, P. Toczek, and V. Vaskonen, Primordial black holes from strong first-order phase transitions, J. High Energy Phys. 09 (2023) 092.
[41] T. C. Gehrman, B. Shams Es Haghi, K. Sinha, and T. Xu, Recycled dark matter, J. Cosmol. Astropart. Phys. 03 (2024) 044.
[42] T. Kim, P. Lu, D. Marfatia, and V. Takhistov, Regurgitated dark matter, arXiv:2309.05703.
[43] S. W. Hawking, Black holes from cosmic strings, Phys. Lett. B **231**, 237 (1989).
[44] H. Deng, J. Garriga, and A. Vilenkin, Primordial black hole and wormhole formation by domain walls, J. Cosmol. Astropart. Phys. 04 (2017) 050.
[45] R. Anantua, R. Easther, and J. T. Giblin, GUT-scale primordial black holes: Consequences and constraints, Phys. Rev. Lett. **103**, 111303 (2009).
[46] J. L. Zagorac, R. Easther, and N. Padmanabhan, GUT-scale primordial black holes: Mergers and gravitational waves, J. Cosmol. Astropart. Phys. 06 (2019) 052.
[47] R. Saito and J. Yokoyama, Gravitational wave background as a probe of the primordial black hole abundance, Phys. Rev. Lett. **102**, 161101 (2009); **107**, 069901(E) (2011).
[48] K. Inomata, M. Kawasaki, K. Mukaida, T. Terada, and T. T. Yanagida, Gravitational wave production right after a primordial black hole evaporation, Phys. Rev. D **101**, 123533 (2020).
[49] T. Papanikolaou, V. Vennin, and D. Langlois, Gravitational waves from a universe filled with primordial black holes, J. Cosmol. Astropart. Phys. 03 (2021) 053.
[50] G. Domènech, C. Lin, and M. Sasaki, Gravitational wave constraints on the primordial black hole dominated early universe, J. Cosmol. Astropart. Phys. 04 (2021) 062; 11 (2021) E01.
[51] G. Domènech, V. Takhistov, and M. Sasaki, Exploring evaporating primordial black holes with gravitational waves, Phys. Lett. B **823**, 136722 (2021).
[52] T. C. Gehrman, B. Shams Es Haghi, K. Sinha, and T. Xu, The primordial black holes that disappeared: Connections to dark matter and MHz-GHz gravitational waves, J. Cosmol. Astropart. Phys. 10 (2023) 001.
[53] K.-P. Xie, Pinning down the primordial black hole formation mechanism with gamma-rays and gravitational waves, J. Cosmol. Astropart. Phys. 06 (2023) 008.
[54] I. K. Banerjee and U. K. Dey, Probing the origin of primordial black holes through novel gravitational wave spectrum, J. Cosmol. Astropart. Phys. 07 (2023) 024.
[55] I. Baldes and M. O. Olea-Romacho, Primordial black holes as dark matter: Interferometric tests of phase transition origin, J. High Energy Phys. 01 (2024) 133.
[56] I. K. Banerjee and U. K. Dey, Gravitational wave probe of primordial black hole origin via superradiance, J. Cosmol. Astropart. Phys. 04 (2024) 049.
[57] Y. Gouttenoire, Primordial black holes from conformal Higgs, Phys. Lett. B **855**, 138800 (2024).
[58] S. Kawamura *et al.*, The Japanese space gravitational wave antenna DECIGO, Classical Quantum Gravity **23**, S125 (2006).
[59] K. Yagi and N. Seto, Detector configuration of DECIGO/BBO and identification of cosmological neutron-star binaries, Phys. Rev. D **83**, 044011 (2011); **95**, 109901(E) (2017).
[60] M. Punturo *et al.* (ET Collaboration), The Einstein telescope: A third-generation gravitational wave observatory, Classical Quantum Gravity **27**, 194002 (2010).
[61] B. P. Abbott *et al.* (LIGO Scientific Collaboration), Exploring the sensitivity of next generation gravitational wave detectors, Classical Quantum Gravity **34**, 044001 (2017).
[62] S. Sato *et al.*, The status of DECIGO, J. Phys. Conf. Ser. **840**, 012010 (2017).
[63] T. Ishikawa *et al.*, Improvement of the target sensitivity in DECIGO by optimizing its parameters for quantum noise including the effect of diffraction loss, Galaxies **9**, 14 (2021).
[64] D. Marfatia and P.-Y. Tseng, Correlated signals of first-order phase transitions and primordial black hole

evaporation, J. High Energy Phys. 08 (2022) 001; 08 (2022) 249(E).
[65] P.-Y. Tseng and Y.-M. Yeh, 511 keV line and primordial black holes from first-order phase transitions, J. Cosmol. Astropart. Phys. 08 (2023) 035.
[66] P. Lu, K. Kawana, and A. Kusenko, Late-forming primordial black holes: Beyond the CMB era, Phys. Rev. D **107**, 103037 (2023).
[67] D. Marfatia and P.-Y. Tseng, Boosted dark matter from primordial black holes produced in a first-order phase transition, J. High Energy Phys. 04 (2023) 006.
[68] S. R. Coleman and E. J. Weinberg, Radiative corrections as the origin of spontaneous symmetry breaking, Phys. Rev. D **7**, 1888 (1973).
[69] L. Dolan and R. Jackiw, Symmetry behavior at finite temperature, Phys. Rev. D **9**, 3320 (1974).
[70] M. Quiros, Finite temperature field theory and phase transitions, in *Proceedings of the ICTP Summer School in High-Energy Physics and Cosmology* (1999), pp. 187–259; arXiv:hep-ph/9901312.
[71] P. Fendley, The effective potential and the coupling constant at high temperature, Phys. Lett. B **196**, 175 (1987).
[72] R. R. Parwani, Resummation in a hot scalar field theory, Phys. Rev. D **45**, 4695 (1992); **48**, 5965(E) (1993).
[73] P. B. Arnold and O. Espinosa, The effective potential and first order phase transitions: Beyond leading-order, Phys. Rev. D **47**, 3546 (1993); **50**, 6662(E) (1994).
[74] A. D. Linde, Fate of the false vacuum at finite temperature: Theory and applications, Phys. Lett. **100B**, 37 (1981).
[75] J. Ellis, M. Lewicki, and J. M. No, On the maximal strength of a first-order electroweak phase transition and its gravitational wave signal, J. Cosmol. Astropart. Phys. 04 (2019) 003.
[76] J. Ellis, M. Lewicki, and V. Vaskonen, Updated predictions for gravitational waves produced in a strongly supercooled phase transition, J. Cosmol. Astropart. Phys. 11 (2020) 020.
[77] C. Caprini *et al.*, Detecting gravitational waves from cosmological phase transitions with LISA: An update, J. Cosmol. Astropart. Phys. 03 (2020) 024.
[78] D. Borah, A. Dasgupta, K. Fujikura, S. K. Kang, and D. Mahanta, Observable gravitational waves in minimal scotogenic model, J. Cosmol. Astropart. Phys. 08 (2020) 046.
[79] M. Kamionkowski, A. Kosowsky, and M. S. Turner, Gravitational radiation from first order phase transitions, Phys. Rev. D **49**, 2837 (1994).
[80] P. J. Steinhardt, Relativistic detonation waves and bubble growth in false vacuum decay, Phys. Rev. D **25**, 2074 (1982).
[81] J. R. Espinosa, T. Konstandin, J. M. No, and G. Servant, Energy budget of cosmological first-order phase transitions, J. Cosmol. Astropart. Phys. 06 (2010) 028.
[82] M. Lewicki, M. Merchand, and M. Zych, Electroweak bubble wall expansion: Gravitational waves and baryogenesis in standard model-like thermal plasma, J. High Energy Phys. 02 (2022) 017.
[83] F. C. Adams, General solutions for tunneling of scalar fields with quartic potentials, Phys. Rev. D **48**, 2800 (1993).
[84] D. Borah, A. Dasgupta, and I. Saha, Leptogenesis and dark matter through relativistic bubble walls with observable gravitational waves, J. High Energy Phys. 11 (2022) 136.
[85] T. D. Lee and Y. Pang, Fermion soliton stars and black holes, Phys. Rev. D **35**, 3678 (1987).
[86] J.-P. Hong, S. Jung, and K.-P. Xie, Fermi-ball dark matter from a first-order phase transition, Phys. Rev. D **102**, 075028 (2020).
[87] L. Del Grosso, G. Franciolini, P. Pani, and A. Urbano, Fermion soliton stars, Phys. Rev. D **108**, 044024 (2023).
[88] M. S. Turner and F. Wilczek, Relic gravitational waves and extended inflation, Phys. Rev. Lett. **65**, 3080 (1990).
[89] A. Kosowsky, M. S. Turner, and R. Watkins, Gravitational radiation from colliding vacuum bubbles, Phys. Rev. D **45**, 4514 (1992).
[90] A. Kosowsky, M. S. Turner, and R. Watkins, Gravitational waves from first order cosmological phase transitions, Phys. Rev. Lett. **69**, 2026 (1992).
[91] A. Kosowsky and M. S. Turner, Gravitational radiation from colliding vacuum bubbles: Envelope approximation to many bubble collisions, Phys. Rev. D **47**, 4372 (1993).
[92] M. S. Turner, E. J. Weinberg, and L. M. Widrow, Bubble nucleation in first order inflation and other cosmological phase transitions, Phys. Rev. D **46**, 2384 (1992).
[93] M. Hindmarsh, S. J. Huber, K. Rummukainen, and D. J. Weir, Gravitational waves from the sound of a first order phase transition, Phys. Rev. Lett. **112**, 041301 (2014).
[94] J. T. Giblin and J. B. Mertens, Gravitional radiation from first-order phase transitions in the presence of a fluid, Phys. Rev. D **90**, 023532 (2014).
[95] M. Hindmarsh, S. J. Huber, K. Rummukainen, and D. J. Weir, Numerical simulations of acoustically generated gravitational waves at a first order phase transition, Phys. Rev. D **92**, 123009 (2015).
[96] M. Hindmarsh, S. J. Huber, K. Rummukainen, and D. J. Weir, Shape of the acoustic gravitational wave power spectrum from a first order phase transition, Phys. Rev. D **96**, 103520 (2017); **101**, 089902(E) (2020).
[97] A. Kosowsky, A. Mack, and T. Kahniashvili, Gravitational radiation from cosmological turbulence, Phys. Rev. D **66**, 024030 (2002).
[98] C. Caprini and R. Durrer, Gravitational waves from stochastic relativistic sources: Primordial turbulence and magnetic fields, Phys. Rev. D **74**, 063521 (2006).
[99] G. Gogoberidze, T. Kahniashvili, and A. Kosowsky, The spectrum of gravitational radiation from primordial turbulence, Phys. Rev. D **76**, 083002 (2007).
[100] C. Caprini, R. Durrer, and G. Servant, The stochastic gravitational wave background from turbulence and magnetic fields generated by a first-order phase transition, J. Cosmol. Astropart. Phys. 12 (2009) 024.
[101] P. Niksa, M. Schlederer, and G. Sigl, Gravitational waves produced by compressible MHD turbulence from cosmological phase transitions, Classical Quantum Gravity **35**, 144001 (2018).
[102] C. Caprini *et al.*, Science with the space-based interferometer eLISA. II: Gravitational waves from cosmological phase transitions, J. Cosmol. Astropart. Phys. 04 (2016) 001.
[103] H.-K. Guo, K. Sinha, D. Vagie, and G. White, Phase transitions in an expanding universe: Stochastic gravitational waves in standard and non-standard histories, J. Cosmol. Astropart. Phys. 01 (2021) 001.

[104] D. Hooper, G. Krnjaic, J. March-Russell, S. D. McDermott, and R. Petrossian-Byrne, Hot gravitons and gravitational waves from Kerr black holes in the early universe, arXiv:2004.00618.
[105] G. Domènech, Scalar induced gravitational waves review, Universe **7**, 398 (2021).
[106] T. Papanikolaou, Gravitational waves induced from primordial black hole fluctuations: The effect of an extended mass function, J. Cosmol. Astropart. Phys. 10 (2022) 089.
[107] D. Borah, S. Jyoti Das, R. Samanta, and F. R. Urban, PBH-infused seesaw origin of matter and unique gravitational waves, J. High Energy Phys. 03 (2023) 127.
[108] A. Weltman *et al.*, Fundamental physics with the square kilometre array, Pub. Astron. Soc. Aust. **37**, e002 (2020).
[109] J. Garcia-Bellido, H. Murayama, and G. White, Exploring the early universe with gaia and THEIA, J. Cosmol. Astropart. Phys. 12 (2021) 023.
[110] A. Sesana *et al.*, Unveiling the gravitational universe at μ-Hz frequencies, Exper. Astron. **51**, 1333 (2021).
[111] P. Amaro-Seoane *et al.* (LISA Collaboration), Laser interferometer space antenna, arXiv:1702.00786.
[112] Y. A. El-Neaj *et al.* (AEDGE Collaboration), AEDGE: Atomic experiment for dark matter and gravity exploration in space, Eur. Phys. J. Quantum Technol. **7**, 6 (2020).
[113] J. Aasi *et al.* (LIGO Scientific Collaboration), Advanced LIGO, Classical Quantum Gravity **32**, 074001 (2015).
[114] R. Samanta and F. R. Urban, Testing super heavy dark matter from primordial black holes with gravitational waves, J. Cosmol. Astropart. Phys. 06 (2022) 017.
[115] M. J. Baker, J. Kopp, and A. J. Long, Filtered dark matter at a first order phase transition, Phys. Rev. Lett. **125**, 151102 (2020).
[116] G. Domènech and M. Sasaki, Gravitational wave hints black hole remnants as dark matter, Classical Quantum Gravity **40**, 177001 (2023).
[117] I. Masina, Dark matter and dark radiation from evaporating primordial black holes, Eur. Phys. J. Plus **135**, 552 (2020).
[118] N. Bernal and O. Zapata, Self-interacting dark matter from primordial black holes, J. Cosmol. Astropart. Phys. 03 (2021) 007.
[119] V. Iršič *et al.*, New constraints on the free-streaming of warm dark matter from intermediate and small scale Lyman-α forest data, Phys. Rev. D **96**, 023522 (2017).
[120] G. Ballesteros, M. A. G. Garcia, and M. Pierre, How warm are non-thermal relics? Lyman-α bounds on out-of-equilibrium dark matter, J. Cosmol. Astropart. Phys. 03 (2021) 101.
[121] F. D'Eramo and A. Lenoci, Lower mass bounds on FIMP dark matter produced via freeze-in, J. Cosmol. Astropart. Phys. 10 (2021) 045.
[122] R. Diamanti, S. Ando, S. Gariazzo, O. Mena, and C. Weniger, Cold dark matter plus not-so-clumpy dark relics, J. Cosmol. Astropart. Phys. 06 (2017) 008.
[123] I. Musco, J. C. Miller, and L. Rezzolla, Computations of primordial black hole formation, Classical Quantum Gravity **22**, 1405 (2005).
[124] K. Kawana, T. Kim, and P. Lu, PBH formation from overdensities in delayed vacuum transitions, Phys. Rev. D **108**, 103531 (2023).
[125] K. Hashino, S. Kanemura, T. Takahashi, and M. Tanaka, Probing first-order electroweak phase transition via primordial black holes in the effective field theory, Phys. Lett. B **838**, 137688 (2023).
[126] T. H. Jung and T. Okui, Primordial black holes from bubble collisions during a first-order phase transition, arXiv:2110.04271.
[127] N. Aggarwal *et al.*, Challenges and opportunities of gravitational wave searches at MHz to GHz frequencies, Living Rev. Relativity **24**, 4 (2021).
[128] D. Chway, T. H. Jung, and C. S. Shin, Dark matter filtering-out effect during a first-order phase transition, Phys. Rev. D **101**, 095019 (2020).